Intermediate-spin ferrous iron in lowermost mantle post-perovskite and perovskite

JUNG-FU LIN[1]*, HEATHER WATSON[2], GYÖRGY VANKÓ[3], ESEN E. ALP[4], VITALI B. PRAKAPENKA[5], PRZEMEK DERA[5], VIKTOR V. STRUZHKIN[6], ATSUSHI KUBO[5], JIYONG ZHAO[4], CATHERINE McCAMMON[7] AND WILLIAM J. EVANS[2]

[1]Department of Geological Sciences, Jackson School of Geosciences, The University of Texas at Austin, Texas 78712, USA
[2]Lawrence Livermore National Laboratory, 7000 East Avenue, Livermore, California 94550, USA
[3]KFKI Research Institute for Particle and Nuclear Physics, PO Box 49, H-1525 Budapest, Hungary
[4]Advanced Photon Source, Argonne National Laboratory, 9700 South Cass Avenue, Argonne, Illinois 60439, USA
[5]Consortium for Advanced Radiation Sources, The University of Chicago, Chicago, Illinois 60637, USA
[6]Geophysical Laboratory, Carnegie Institution of Washington, 5251 Broad Branch Rd. NW, Washington, DC 20015, USA
[7]Bayerisches Geoinstitut, Universität Bayreuth, D-95440 Bayreuth, Germany
*e-mail: afu@jsg.utexas.edu

Published online: 14 September 2008; doi:10.1038/ngeo310

Iron-bearing silicate post-perovskite and perovskite are believed to be the dominant minerals of the lowermost mantle and the lower mantle, respectively. The electronic spin state of iron—a quantum property of every electron associated with its angular momentum—can strongly influence the properties of these mineral phases and thereby the nature of the Earth's interior[1–15]. However, the spin state of iron at lowermost-mantle pressure/temperature conditions is poorly known[16–27]. Here we use *in situ* X-ray emission, X-ray diffraction and synchrotron Mössbauer spectroscopic techniques to measure the spin and valence states of iron in post-perovskite and perovskite at conditions relevant to the lowermost mantle[25,28]. We find that Fe^{2+} exists predominantly in the intermediate-spin state with a total spin number of one in both phases. We conclude that changes in the radiative thermal conductivity and iron partitioning in the lowermost mantle would thus be controlled by the structural transition from perovskite to post-perovskite, rather than the electronic transition of Fe^{2+}.

Deep-mantle investigations over the past decade show that the approximately 100–350-km-thick D″ layer located just above the core–mantle boundary is generally characterized by strong seismic discontinuities[1–4]. Recent discovery of the silicate perovskite [$(Mg, Fe)SiO_3$] to silicate post-perovskite transition[5,6] at pressure–temperature conditions relevant to the D″ region has provided new insights into its enigmatic properties, including seismic discontinuities[1–4], rheology and plasticity[7], dynamic evolution and formation of superplumes[8–10], thermal gradients, core–mantle heat flux[11,12], and chemistry[13–15]. Whereas perovskite and post-perovskite phases are believed to be the most abundant minerals of the lower mantle and D″ layer, respectively, a double-crossing transition from post-perovskite to perovskite is suggested to occur at the bottom of the D″ layer[2–4]. Knowledge of the properties of these lowermost-mantle minerals is thus essential to decipher seismic observations, geochemical modelling and geodynamic simulation of the Earth's deep interior. Of particular importance to these issues is the electronic spin and valence states of iron in post-perovskite and perovskite because the partially filled 3*d*-electron orbitals of iron have essential roles in their thermal conductivity, electrical conductivity and iron partitioning, among other properties[16].

Electronic spin-pairing transitions of iron have recently been reported to occur in lower-mantle ferropericlase and perovskite at high pressures and/or high temperatures[16–27]. These results affect our understanding of the geophysics and geodynamics of the Earth's lower mantle because the spin transition of iron results in significant changes in density, incompressibility, sound velocities, radiative thermal conductivity and electrical conductivity in ferropericlase. Furthermore, drastic reduction in sound velocities and elastic moduli within the spin transition is reported (see ref. 16 for a recent review). Recent mounting evidence shows that a high-spin to low-spin transition zone in ferropericlase occurs in the middle part of the lower mantle[25], that is, from approximately 1,000 km in depth to 2,200 km in depth, whereas data complementary to the present work show the occurrence of a high-spin to intermediate-spin transition of Fe^{2+} in perovskite at approximately 30 GPa (ref. 26). However, theoretical calculations have indicated that the intermediate-spin state is mostly unstable in perovskite at lower-mantle pressures[21–23,27]. Most importantly, the spin state of iron in the dominant post-perovskite and perovskite has not yet been probed experimentally under relevant pressure–temperature conditions of the lowermost mantle.

Here we have studied the electronic spin states of iron in post-perovskite and perovskite [$(Mg_{0.6}, Fe_{0.4})SiO_3$] and their crystal structures under relevant lowermost-mantle pressure–temperature conditions using *in situ* X-ray emission spectroscopy (XES), synchrotron Mössbauer spectroscopy (SMS) and X-ray diffraction in a laser-heated diamond-anvil cell[25,28] (DAC) (see Supplementary Information, Fig. S1). The starting samples were polycrystalline enstatite [$(Mg_{0.6}, Fe_{0.4})SiO_3$], which was probed by X-ray diffraction and electron microprobe. Mössbauer analyses showed that iron is mainly Fe^{2+} in the high-spin state and there is no evidence of Fe^{3+} in the sample (see Supplementary Information,

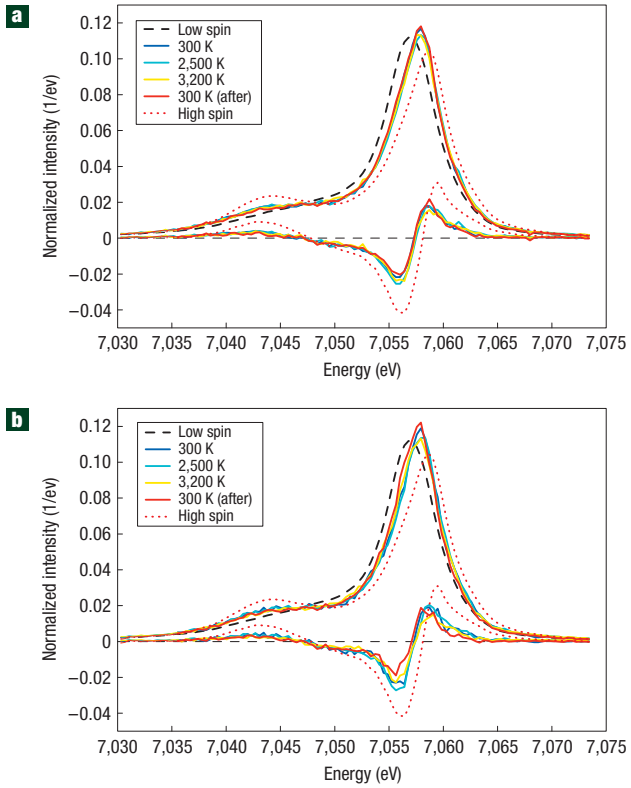

Figure 1 X-ray emission spectra of iron. a, Post-perovskite at 134 GPa. **b**, Perovskite at 108 GPa. High-spin and low-spin references are used for the integrated absolute difference analysis[30], and differences from the low-spin line shape, shown below the spectra, are used to derive the average spin number of Fe^{2+}. An energy shift of 0.8 eV in the main Kβ emission peak, which is approximately half of the energy shift in the high-spin to low-spin transition in ferropericlase[25], is also used to derive the total spin number[30], providing further evidence for the occurrence of the intermediate-spin state.

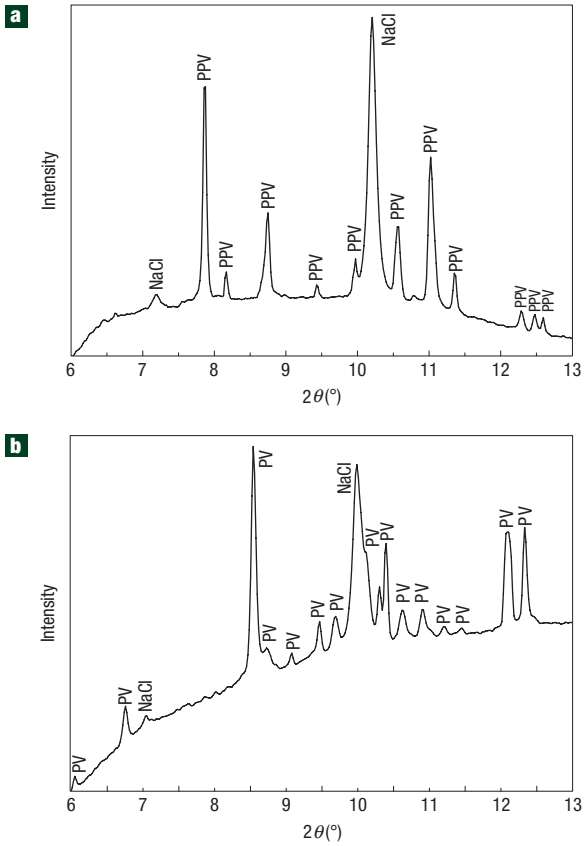

Figure 2 Representative X-ray diffraction patterns. a,**b**, The diffraction patterns of post-perovskite at 134 GPa (**a**) and perovskite at 108 GPa (**b**) were integrated with the FIT2D program, and the backgrounds were not subtracted. PPV, post-perovskite; PV, perovskite; NaCl, thermal insulator and pressure calibrant in the B2 structural phase[29]. Unit-cell parameters of post-perovskite at 134 GPa are $a = 2.456$ Å (±0.002), $b = 8.118$ Å (±0.005), $c = 6.099$ Å (0.003) and $V = 121.58$ Å^3 (±0.03), whereas unit-cell parameters of perovskite at 108 GPa are $a = 4.394$ Å (±0.006), $b = 4.572$ Å (±0.008), $c = 6.349$ Å (0.008) and $V = 127.55$ Å^3 (±0.05).

Fig. S2). The higher iron content in the sample allowed us to laser-heat the sample consistently for a long time and to collect the XES and SMS spectra within a reasonable time frame. Samples approximately 15 μm thick and 40–50 μm in diameter were loaded into DACs with 100–300 μm bevel diamonds, Be gaskets of 3 mm in diameter and cubic BN gasket inserts. Samples were sandwiched between dried NaCl layers in the DACs, and the NaCl was used as the thermal insulators, pressure medium and pressure calibrant[29] (see Supplementary Information, Fig. S1).

In situ high pressure–temperature XES and X-ray diffraction experiments were conducted at the GeoSoilEnviroCARS sector of the Advanced Photon Source (APS), Argonne National Laboratory (ANL) using a Rowland circle spectrometer configured around the double-sided laser-heating system[25], whereas the SMS spectra of these samples were collected at high pressures and room temperature at XOR-3 of the APS, ANL (ref. 28). The enstatite samples in the DACs were compressed to 108 GPa and 134 GPa and laser-heated at approximately 2,500 K to 3,000 K for at least 3 h to be fully transformed to perovskite and post-perovskite phases, respectively.

XES spectra of the Fe Kβ fluorescence lines and X-ray diffraction patterns were collected up to 3,200 K in post-perovskite at 134 GPa and in perovskite at 108 GPa (Figs 1 and 2). The *in situ* X-ray diffraction patterns of samples revealed single post-perovskite phase at 134 GPa and perovskite phase at 108 GPa respectively, without any sign of other phases (except the NaCl pressure standard). XES spectra of the enstatite were also collected at ambient conditions and 108 GPa before the sample was laser-heated. These spectra, together with high-spin/low-spin ferropericlase and Fe^{2+}-containing molecules, were used as references to quantitatively derive the total local spin number of iron using integrated absolute difference analysis, and the peak position of the Fe Kβ peak, which is independent of the reference spectra used and the integrated absolute difference analysis, provides further evidence for the total spin number of iron in the samples[30] (Fig. 3; Supplementary Information, Figs S3,S4).

The derived spin number of iron from 300 to 3,200 K in post-perovskite at 134 GPa and in perovskite at 108 GPa is consistent with an average number of one and high temperatures do not cause significant variation of this value (Fig. 3). SMS spectra show that perovskite exhibits two iron sites both with extremely high quadrupole splitting of 4–4.2 mm s^{-1} and relatively high centre shifts at 110 GPa, and post-perovskite at 134 GPa is also dominated by two iron sites with extremely high quadrupole splitting and relatively high centre shift (Fig. 4, Supplementary Information, Fig. S3, Table S1). We note that high-spin Fe^{2+}

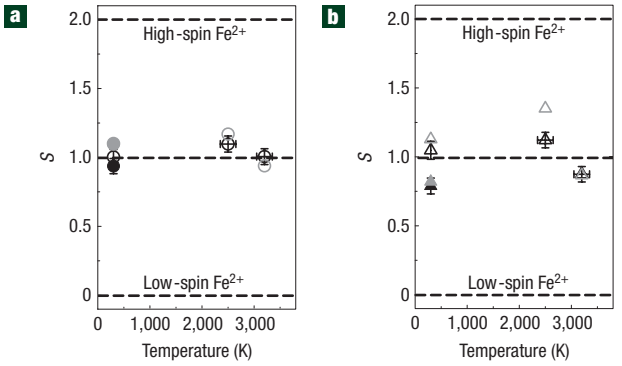

Figure 3 Average spin number of Fe^{2+}. a, Post-perovskite at 134 GPa. **b**, Perovskite at 108 GPa. The average spin number (S), plotted as a function of temperature, is derived from the integrated absolute difference analysis of the XES spectra of the samples and the high-spin/low-spin references (black symbols) or the shift of the Kβ peak position (grey symbols) (Fig. 1, Supplementary Information, Fig. S4). Solid symbols represent the spin number derived from the XES spectra of the samples after two days of laser-heating. Temperature uncertainties in the laser-heating experiments were approximately 150 K.

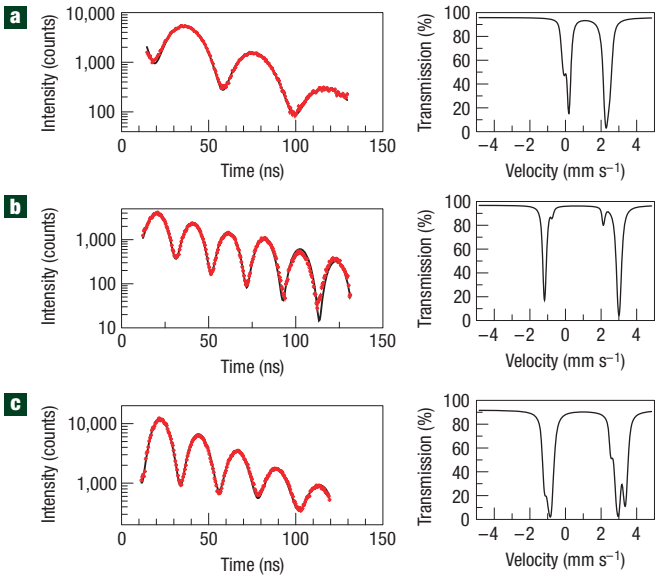

Figure 4 Representative synchrotron Mössbauer spectra. a, Enstatite at ambient conditions. **b**, Silicate perovskite at 110 GPa. **c**, Silicate post-perovskite at 134 GPa. Corresponding energy spectra calculated from the fits are shown in the left panels. Both perovskite and post-perovskite exhibit very high quadrupole splitting and centre shift. Red circles: experimental SMS spectra; black lines: modelled spectra. The perovskite spectrum is fitted to two iron sites with quadrupole splitting of 4.0–4.2 mm s^{-1} and centre shift of 0.84–0.97 mm s^{-1}. The post-perovskite spectrum is fitted to a three-site model with two sites (90% abundance) with quadrupole splitting of 3.8–4.5 mm s^{-1} and centre shift of 0.95–1.00 mm s^{-1}.

has quadrupole splitting values of 2–3 mm s^{-1} and high-spin Fe^{3+} has extremely low quadrupole splitting in perovskite at high pressures[26]. Using both the XES and SMS results, we can thus rule out the possibility that the averaged total spin number of one is a result of mixed-spin states in which half of the high-spin Fe^{2+} transforms to the low-spin state (Fig. 3). Together with a complementary high-pressure Mössbauer study that observed a new dominant quadrupole doublet with extremely high quadrupole splitting, relatively high centre shift and narrow linewidth above ~30 GPa in perovskite[26], our XES and SMS results strongly support the conclusion that iron predominantly exists in Fe^{2+} with a single 3d electronic state of $S = 1$ in our post-perovskite and perovskite samples at pressure–temperature conditions of the lowermost mantle (see Supplementary Information, Figs S5,S6). The iron content of 40% (or 8 mol%) in our samples is probably below the percolation threshold where the effect of the iron–iron interaction is generally too small to have any significant effect on the spin transition pressure. Thus, Fe^{2+} in silicate perovskite and post-perovskite with an iron content close to the modelled lower-mantle composition such as $(Mg_{0.9}, Fe_{0.1})SiO_3$ would be in the intermediate-spin state under lowermost-mantle conditions. The $S = 1$ state of Fe^{2+} is called the intermediate-spin state here for historical reasons[18,26] (see Supplementary Information, Fig. S5). We note that previous high-pressure studies used samples with unspecified Fe^{3+} content[17] or very high Fe^{3+} content of 40–70% in perovskite[18,19]. The high Fe^{3+} content, together with the metastability of perovskite under non-hydrostatic conditions and different annealing history in high-pressure DACs, probably contributes to the complexity of recent reports on the spin states of iron in perovskite. Specifically, the lower Kβ' satellite intensity in a perovskite sample at 132–145 GPa could be the result of compression under non-hydrostatic conditions at room temperature, as suggested by our enstatite sample which became amorphous and lost its spin momentum completely at 108 GPa after compression at 300 K (see Supplementary Information, Fig. S4).

Perovskite and post-perovskite exhibit very high degrees of lattice distortion at high pressures, which would contribute to the stabilization of the intermediate-spin Fe^{2+} through strong Jahn–Teller distortions that increase the splitting of the upper level 3d orbitals[26] (see Supplementary Information, Fig. S5). This may explain the discrepancy between our observation and theoretical and thermodynamic predictions, in which the intermediate-spin state is unstable at lowermost-mantle pressures[21–23,27]. As the high-spin to intermediate-spin transition is observed to occur at approximately 30 GPa and room temperature and intermediate-spin Fe^{2+} exists over an extended temperature range[26], particularly at lowermost-mantle pressures and temperatures in perovskite (see Supplementary Information, Fig. S6), a spin transition zone from high-spin to intermediate-spin state probably occurs in the uppermost lower mantle in perovskite. With the knowledge that a high-spin to low-spin transition zone occurs in ferropericlase in the middle part of the lower mantle[25], it remains to be seen how this spin transition in perovskite interacts with the spin transition in ferropericlase and in turn may have an effect on the physical and chemical properties of the lower mantle.

The observation of the intermediate-spin Fe^{2+} in both post-perovskite and perovskite near the D″ region has important geodynamic and geochemical ramifications. Owing to the predominant abundance of post-perovskite and perovskite in the lowermost mantle, their thermal conductivities would have a strong influence on the formation of superplumes, temperature gradients and thermal evolution of the mantle and the core[8–12]. Because of the partially filled 3d-electron orbitals that exhibit a bandgap in the electronvolt range, the electronic states of iron strongly govern the radiative thermal conductivity, electrical conductivity and iron partitioning in these minerals[16]. Our studies show that both perovskite and post-perovskite accommodate the same intermediate-spin Fe^{2+} and that their opacity and

absorption behaviour in the infrared wavelength range are very similar in our high pressure–temperature experiments. These indicate that corresponding changes in the radiative thermal conductivity, electrical conductivity and iron partitioning would be due to the crystal structural transition, rather than the electronic spin transition, from perovskite to post-perovskite; although, the spin state of Fe^{3+} and its effects in these phases remain to be understood.

Recent geodynamic modelling of the lower mantle showed that even extremely large increases of the radiative thermal conductivity cannot inhibit mantle mixing, and may even enhance mantle mixing, and that reasonable increases in the radiative thermal conductivity can lead to larger, more stable plumes in the convecting mantle[8–10]. In light of our observations here, changes in the radiative thermal conductivity in the D″ region are unlikely to have a dominant role in mantle convection and formation of superplumes. This suggests that other mechanisms such as compositionally dense and hot chemical piles may be responsible for controlling the formation of superplumes. Furthermore, the overall temperature gradient and magnitude across the double-crossing of the lowermost mantle should be smaller than what is expected with a significant change in the thermal conductivity at the D″ region[11,17]. It remains to be further investigated what influence the intermediate-spin post-perovskite and perovskite would have on our knowledge of the thermal and dynamic evolution of the core, as the heat flux and thermal history from the core to the mantle are significantly governed by the thermal conductivity of the lowermost-mantle minerals.

METHODS

Two diode-pumped ytterbium infrared fibre lasers were focused down to flat-top shapes of 25 μm in diameter at the sample position and were used to laser-heat the sample from both sides of the DAC. A monochromatic beam with wavelength of 0.3344 Å was used as the X-ray source and the diffracted X-rays were collected by a CCD (charge-coupled device; MAR165). The X-ray diffraction measurements were used to confirm the crystal structures of our samples at high pressures. Temperatures were measured from the thermal radiation spectra fitted to the Planck radiation function. A monochromatic X-ray beam of 14 keV was focused down to approximately 5 μm vertically and horizontally at the sample position in the XES experiments. The Fe Kβ emission spectra were collected by a silicon detector through the Be gasket and a Si analyser in the Rowland circle geometry. During the laser-heated XES experiments, we also double-checked the crystal structures of the samples by tuning the monochromatic X-ray beam from 14 to 25 keV and collected X-ray diffraction patterns. Monitoring the perovskite and post-perovskite synthesis process as a function of time using X-ray diffraction showed that prolonged laser-heating of the samples at 2,500–3,000 K was needed to completely transform the enstatite samples to post-perovskite at 134 GPa and perovskite at 108 GPa, respectively.

In the SMS experiments, a monochromatic X-ray beam of ~14.4125 keV with 1 meV resolution and 15 μm in diameter at XOR-3 was used to excite the nuclear resonance of the ^{57}Fe nuclei in the sample[28]. The time-delayed SMS spectra were recorded by an avalanche photodiode detector in the forward direction. After the SMS spectrum of the sample had been collected, a thin stainless-steel foil ($Fe_{55}Cr_{20}Ni_{25}$) of 0.538 μm in thickness was placed outside the DAC to serve as a reference for the centre-shift measurements. The SMS spectra were evaluated with the CONUSS programs[28] to derive the hyperfine parameters, quadrupole splitting and centre shift. The same perovskite and post-perovskite samples were used for all XES, SMS and diffraction experiments, enabling us to cross-check their crystal structures, total 3*d* spin number (momentum) (*S*) and spin and valence states of iron in the samples. The details of the experimental set-up, sample synthesis and analyses are reported in Supplementary Information.

Received 7 May 2008; accepted 19 August 2008; published 14 September 2008.

References

1. Garnero, E. J., Maupin, V., Lay, T. & Fouch, M. J. Variable azimuthal anisotropy in Earth's lowermost mantle. *Science* **306**, 259–261 (2004).
2. Hernlund, J. W., Thomas, C. & Tackley, P. J. A doubling of the post-perovskite phase boundary and structure of the Earth's lowermost mantle. *Nature* **434**, 882–886 (2005).
3. Lay, T., Hernlund, J., Garnero, E. J. & Thorne, M. S. A post-perovskite lens and D″ heat flux beneath the central Pacific. *Science* **314**, 1272–1276 (2006).
4. van der Hilst, R. D. *et al.* Seismostratigraphy and thermal structure of Earth's core-mantle boundary region. *Science* **315**, 1813–1817 (2007).
5. Murakami, M., Hirose, K., Kawamura, K., Sata, N. & Ohishi, Y. Post-perovskite phase transition in $MgSiO_3$. *Science* **304**, 855–858 (2004).
6. Oganov, A. R. & Ono, S. Theoretical and experimental evidence for a post-perovskite phase of $MgSiO_3$ in Earth's D″ layer. *Nature* **430**, 445–448 (2004).
7. Merkel, S. *et al.* Plastic deformation of $MgGeO_3$ post-perovskite at lower mantle pressures. *Science* **311**, 644–646 (2006).
8. Matyska, C. & Yuen, D. A. The importance of radiative heat transfer on superplumes in the lower mantle with the new post-perovskite phase change. *Earth Planet. Sci. Lett.* **234**, 71–81 (2005).
9. Matyska, C. & Yuen, D. A. Lower mantle dynamics with the post-perovskite phase change, radiative thermal conductivity, temperature- and depth-dependent viscosity. *Phys. Earth Planet. Inter.* **154**, 196–207 (2006).
10. Naliboff, J. B. & Kellogg, L. H. Dynamic effects of a step-wise increase in thermal conductivity and viscosity in the lowermost mantle. *Geophys. Res. Lett.* **33**, L12S09 (2006).
11. Buffett, B. A bound on heat flow below a double crossing of the perovskite-postperovskite phase transition. *Geophys. Res. Lett.* **34**, L17302 (2007).
12. Hofmeister, A. M. & Yuen, D. A. Critical phenomena in thermal conductivity: Implications for lower mantle dynamics. *J. Geodyn.* **44**, 186–199 (2007).
13. Mao, W. L. *et al.* Ferromagnesian postperovskite silicates in the D″ layer of the Earth. *Proc. Natl Acad. Sci. USA* **101**, 15867–15869 (2004).
14. Kobayashi, Y. *et al.* Fe–Mg partitioning between $(Mg, Fe)SiO_3$ post-perovskite, perovskite, and magnesiowüstite in the Earth's lower mantle. *Geophys. Res. Lett.* **32**, L19302 (2005).
15. Murakami, M., Hirose, K., Sata, N. & Ohishi, Y. Post-perovskite phase transition and mineral chemistry in the pyrolitic lowermost mantle. *Geophys. Res. Lett.* **32**, L03304 (2005).
16. Lin, J. F., Jacobsen, S. D. & Wentzcovitch, R. M. Electronic spin transition of iron in the Earth's deep mantle. *Eos Trans. Am. Geophys. Union* **88**, 13–17 (2007).
17. Badro, J. *et al.* Electronic transitions in perovskite: Possible nonconvecting layers in the lower mantle. *Science* **305**, 383–386 (2004).
18. Li, J. *et al.* Electronic spin state of iron in lower mantle perovskite. *Proc. Natl Acad. Sci. USA* **101**, 14027–14030 (2004).
19. Jackson, J. M. *et al.* A synchrotron Mössbauer spectroscopy study of $(Mg, Fe)SiO_3$ perovskite up to 120 GPa. *Am. Mineral.* **90**, 199–205 (2005).
20. Goncharov, A. F., Struzhkin, V. V. & Jacobsen, S. D. Reduced radiative conductivity of low-spin (Mg,Fe)O in the lower mantle. *Science* **312**, 1205–1208 (2006).
21. Stackhouse, S., Brodholt, J., Dobson, D. P. & Price, G. D. Electronic spin transitions and the seismic properties of ferrous iron bearing $MgSiO_3$ post-perovskite. *Geophys. Res. Lett.* **33**, L12S03 (2006).
22. Zhang, F. & Oganov, A. R. Valence state and spin transitions of iron in Earth's mantle silicates. *Earth Planet. Sci. Lett.* **249**, 436–443 (2006).
23. Bengtson, A., Persson, K. & Morgan, D. *Ab initio* study of the composition dependence of the pressure-induced spin transition in the $(Mg_{1-x}, Fe_x)SiO_3$ system. *Earth Planet. Sci. Lett.* **265**, 535–545 (2008).
24. Keppler, H., Kantor, I. & Dubrovinsky, L. S. Optical absorption spectra of ferropericlase to 84 GPa. *Am. Mineral.* **92**, 433–436 (2007).
25. Lin, J. F. *et al.* Spin transition zone in Earth's lower mantle. *Science* **317**, 1740–1743 (2007).
26. McCammon, C. *et al.* Intermediate-spin ferrous iron in lower mantle perovskite. *Nature Geosci.* **1**, 684–687 (2008).
27. Stackhouse, S., Brodholt, J. P. & Price, G. D. Electronic spin transitions in iron-bearing $MgSiO_3$ perovskite. *Earth Planet. Sci. Lett.* **253**, 282–290 (2007).
28. Sturhahn, W. Nuclear resonant spectroscopy. *J. Phys. Condens. Matter* **16**, S497–S530 (2004).
29. Fei, Y. *et al.* Toward an internally consistent pressure scale. *Proc. Natl Acad. Sci. USA* **104**, 9182–9186 (2007).
30. Vankó, G. *et al.* Probing the 3d spin momentum with X-ray emission spectroscopy: The case of molecular-spin transitions. *J. Phys. Chem. B* **110**, 11647–11653 (2006).

Supplementary Information accompanies the paper at www.nature.com/naturegeoscience.

Acknowledgements

We acknowledge GSECARS and XOR-3, APS, ANL for the use of the synchrotron and laser facilities. We thank J. Nalibof, E. J. Garnero, B. Maddox, W. Sturhahn, J. Lassiter and S. Grand for helpful discussions. Use of the Advanced Photon Source was supported by US Department of Energy, Office of Science, Basic Energy Sciences, under contract No. DE-AC02-06CH11357. GSECARS is supported by NSF Earth Sciences (EAR-0622171) and DOE Geosciences (DE-FG02-94ER14466). This work at Lawrence Livermore National Laboratory was carried out under the auspices of the US Department of Energy by Lawrence Livermore National Laboratory under Contract DE-AC52-07NA27344. J.F.L. was partially supported by the Lawrence Livermore Fellowship. G.V. acknowledges financial support from the Hungarian Research Fund (OTKA) under contract No. K72597 and from the Bolyai Fellowship. V.V.S. acknowledges financial support from DOE.

Author contributions

J.F.L., V.B.P., P.D., V.V.S. and A.K. contributed to the X-ray emission experiments, and J.F.L., E.E.A. and J.Z. contributed to the Mössbauer experiments. H.W. synthesized the starting sample. G.V. and E.E.A. contributed to X-ray emission and Mössbauer data analyses, respectively. All authors participated in the writing and revision of the paper.

Author information

Reprints and permission information is available online at http://npg.nature.com/reprintsandpermissions. Correspondence and requests for materials should be addressed to J.-F.L.